2012

Improved low-voltage-ride-through capability of fixed-speed wind turbines using decentralised control of STATCOM with energy storage system

IET GENERATION TRANSMISSION & DISTRIBUTION, HERTFORD, v. 6, n. 8, supl. 4, Part 1-2, pp. 719-730, AUG, 2012

http://www.producao.usp.br/handle/BDPI/36344

Published in IET Generation, Transmission & Distribution
Received on 20th July 2011
Revised on 30th March 2012
doi: 10.1049/iet-gtd.2011.0537

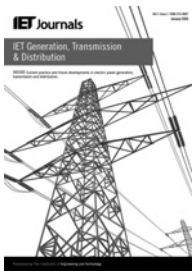

ISSN 1751-8687

Improved low-voltage-ride-through capability of fixed-speed wind turbines using decentralised control of STATCOM with energy storage system

M.J. Hossain[1] *H.R. Pota*[2] *R.A. Ramos*[3]

[1]*Griffith School of Engineering, Griffith University, Gold Coast, QLD-4222, Australia*
[2]*SEIT, UNSW@ADFA, Northcott Drive, Canberra, ACT-2600, Australia*
[3]*Engineering School of Sao Carlos, USP, Av. Trabalhador Sao-carlense, Sao Carlos, Brazil*
E-mail: j.hossain@griffith.edu.au

Abstract: The design and implementation of a new control scheme for reactive power compensation, voltage regulation and transient stability enhancement for wind turbines equipped with fixed-speed induction generators (IGs) in large interconnected power systems is presented in this study. The low-voltage-ride-through (LVRT) capability is provided by extending the range of the operation of the controlled system to include typical post-fault conditions. A systematic procedure is proposed to design decentralised multi-variable controllers for large interconnected power systems using the linear quadratic (LQ) output-feedback control design method and the controller design procedure is formulated as an optimisation problem involving rank-constrained linear matrix inequality (LMI). In this study, it is shown that a static synchronous compensator (STATCOM) with energy storage system (ESS), controlled via robust control technique, is an effective device for improving the LVRT capability of fixed-speed wind turbines.

1 Introduction

Voltage instability is a growing concern for power systems worldwide owing to the increasing impact of induction motor loads, wind turbines and other fast recovering load devices [1]. In this paper, the analysis and control of the response to relatively large perturbations in power systems with wind turbines coupled to squirrel-cage induction generators (SCIG) is considered. Although the use of variable-speed wind turbines with power electronic interfaces is the current trend, many directly connected induction-generator-based wind turbines are still in operation. All wind turbine technologies, irrespective of type, employed in high-power wind farms, are required by new grid codes in some countries to have a fault ride-through capability for faults on the transmission system [2]. To deal with this situation, flexible AC transmission system (FACTS) devices (such as a STATCOM) can be used. However, since STATCOMs are only able to provide reactive power control, their application is limited to reactive power support. As one of the alternatives to overcome this problem, a STATCOM with an energy storage system (STATCOM/ESS) can be used to supply the reactive power, increase the capability to dampen electromechanical oscillations and enhance the low-voltage-ride-through (LVRT) capability of fixed-speed wind turbines. However, although a STATCOM/ESS has great potential to fulfil the requirements of grid code to connect wind turbines, considerable advances in the control of this system are still needed for its practical implementation.

Recently, a control method for limiting the torque and enhance the LVRT capability of grid-connected cage induction machines during the recovery process after grid faults by using a STATCOM is proposed in [3]. The authors in [4] propose a novel damping control algorithm for a STATCOM in a series compensated wind park for mitigating sub-synchronous resonance (SSR) and damping power system oscillations. An efficient control strategy to improve the LVRT capability in doubly fed induction generators (IGs) is proposed in [5]. A proportional-integral (PI)-based voltage and frequency controller is proposed in [6]. The existing control techniques are mainly aimed at maximising the output power, increasing the reactive current during low-voltage, and reducing the peak rotor fault current. However, they do not consider the non-linearity and interactions among wind farms. However, it is essential to consider the non-linearity and interconnection effects in order to design controllers for multi-machine power systems, and also quantify the deviation of the operating point from the equilibrium point for which the system maintains closed-loop stability.

In recent years, the design of robust decentralised controllers for interconnected large power systems has been widely investigated and intensively studied with large attention on guaranteeing the stability of the overall system model in the presence of interconnections terms [7]. Although centralised controllers for such systems can often

be designed using standard control design techniques, centralised control algorithms, in general, require a higher level of connectivity and higher communication costs compared with decentralised schemes. Hence, much effort has been focused on the application of decentralised control in power systems (see [7, 8]). Results concerning robust decentralised control of interconnected power systems – based on approaches that explicitly take into account the interactions terms – have been reported in [9, 10]. In [11], an interesting decentralised turbine/governor controller scheme for power systems has been presented. However, the local state feedback controllers designed using this approach need complete state information (which may not be feasible to obtain). An output-feedback robust decentralised control using linear matrix inequality (LMI) techniques has been presented in [12].

During faults and in post-fault operation, the system state can be significantly far from the desired equilibrium point. In most situations, the post-fault uncontrolled system has unstable post-fault trajectory. The difficulty in providing the LVRT capability is because of the non-linearities in the power system model [13]. Linear controllers have a limited range of operation which normally does not include post-fault voltage conditions [13]. A solution to the LVRT problem is to design globally stabilising controllers [14]. Unfortunately these controllers often need a full-state feedback and are not robust to modelling uncertainties. The next option is to use a linear controller that is robust to the change in the linear model with changing operating conditions – a necessary outcome of the underlying non-linear model.

As mentioned above, robust controllers do exist for power systems but few of them have been able to systematically provide robustness against such large deviations as is required for LVRT. In this paper, we present a method that can be used to design a linear controller that is robust to accommodate post-fault low-voltage conditions. We describe the design of robust decentralised controllers to enhance dynamic voltage and transient stability where instability is caused by a large number of IGs connected in the weak areas of the system. The controller is designed for a stable operation even when the operating point is at a distance from the equilibrium point during transients. The extended robustness is provided by the exact linearisation of the non-linear model using the mean value and the Cauchy remainder [15]. We also include interconnection effects from other machines in the controller design. Prior to the design of the controllers, a modal analysis has been carried out to identify the critical modes and the weakest machines which exert the greatest influence on the instability mechanism. By this approach, the potentially severe perturbations on the system are addressed in the controller design and this makes the proposed design procedure more robust with respect to non-linear behaviours in the system.

The organisation of the paper is as follows: Section 3 provides the mathematical modelling of the power system devices under consideration; test system and control objectives are presented in Section 4; Section 5 describes the linearisation technique and the process for obtaining the bounds on the non-linear terms; Section 6 discusses the decentralised minimax output-feedback controller design procedure using a rank-constrained LMI technique; Section 7 presents the control design algorithm and, in Section 8, the performance of the controller is outlined through a series of non-linear simulation results. Concluding remarks and suggestions for future works are given in Section 9.

2 List of symbols

Symbols in the order in which they appear.

T_{ae}	aerodynamic torque
c_p	power coefficient
R	turbine rotor radius
γ	torsion angle
T_m	mechanical torque
R_r	rotor resistance
X_r	rotor reactance
V_{ds}	d-axis stator voltage
v_{dc}	capacitor voltage
δ	rotor angle
K_m	sensor constant
u	control input
Γ	scaling parameter
v_{sc}	supercapacitor voltage
ρ	air density
λ	tip-speed ratio
H_m, H_G	inertia constant
f	normal grid frequency
ω_G	rotor speed of generator
T'_o	transient time constant
i_{ds}	d-axis stator current
V_{qs}	q-axis stator voltage
E'_{dr}	d-axis transient voltages
α	firing angle of STATCOM
T_m	sensor time constant
y	measured output
$\boldsymbol{\phi}$, $\boldsymbol{\psi}$	uncertainty gain matrix
C_{sc}	supercapacitance
A_{wt}	swept area
θ	pitch angle
K_s	torsion stiffness
T_e	electrical torque
s	slip
X_s	stator reactance
X'	transient reactance
v_t	terminal voltage
C	DC capacitor
m	modulation index
$\boldsymbol{x}$	state vector
ξ	uncertainty input
τ, θ	free parameter
R_s	resistance
ω_m	rotor shaft speed
V_w	wind speed
D_m, D_G	torsion damping
N_g	gear ratio
E'_{qr}	q-axis transient voltages
X	rotor open-circuit reactance
E'_{dr}	d-axis transient voltages

doi: 10.1049/iet-gtd.2011.0537

i_{qs}	q-axis stator current
R_C	internal resistance of C
P_s	input power of STATCOMs
$\boldsymbol{A, B, C, D}$	system matrices
ζ	uncertainty output
k	inverter constant
s_c	critical slip

3 Power system model

Dynamic models of the devices considered in the paper are presented in this section. In this research, the following devices are used: (i) synchronous generators, (ii) fixed-speed wind generators and (iii) STATCOMs with energy storage devices. A single-axis third-order generator model and an IEEE-ST1A type excitation system are used in this paper [16]. A fixed-speed wind generator is mainly equipped with a SCIG. The non-linear model of the wind turbines is based on a static model of the aerodynamics, a two-mass model of the drive train and a third-order model of the IG.

The rotor of the wind turbine, with radius R_i, converts energy from the wind to the rotor shaft, rotating at the speed, ω_{m_i}. The power from the wind depends on the wind speed, V_{w_i}, the air density, ρ_i and the swept area, A_{wt_i}. From the available power in the swept area, the power on the rotor is given based on the power coefficient, $c_{p_i}(\lambda_i, \theta_i)$, which depends on the pitch angle of the blade, θ_i, and the ratio between the speed of the blade tip and the wind speed, denoted tip-speed ratio, $\lambda_i = (\omega_{m_i} R_i / V_{w_i})$. R_i is the wind turbine radius. The aerodynamic torque applied to the rotor for the ith turbine by the effective wind speed passing through the rotor is given as follows [17]

$$T_{ae_i} = \frac{\rho_i}{2\omega_{m_i}} A_{wt_i} c_{p_i}(\lambda_i, \theta_i) V_{w_i}^3 \tag{1}$$

where c_{p_i} is approximated by the following relation [18]

$$c_{p_i} = (0.44 - 0.0167\theta_i) \sin\left[\frac{\pi(\lambda_i - 3)}{15 - 0.3\theta_i}\right] - 0.00184(\lambda_i - 3)\theta_i$$

where $i = 1, \ldots, n$, and n is the number of wind turbines.

The drive train attached to the wind turbine converts the aerodynamic torque T_{ae_i} on the rotor into the torque on the low speed shaft, which is scaled down through the gearbox to the torque on the high-speed shaft. A two-mass drive train model of a wind turbine generator system (WTGS) is used in this paper as drive train modelling can satisfactorily reproduce the dynamic characteristics of the WTGS.

The dynamics of the shaft are represented as [17]

$$\dot{\omega}_{m_i} = \frac{1}{2H_{m_i}} [T_{ae_i} - K_{s_i}\gamma_i - D_{m_i}\omega_{m_i}] \tag{2}$$

$$\dot{\omega}_{G_i} = \frac{1}{2H_{G_i}} [K_{s_i}\gamma_i - T_{e_i} - D_{G_i}\omega_{G_i}] \tag{3}$$

$$\dot{\gamma}_i = 2\pi f \left(\omega_{m_i} - \frac{1}{N_{g_i}}\omega_{G_i}\right) \tag{4}$$

The transient model of an IG is described in this paper by the following equations [17, 19]

$$\dot{s}_i = \frac{1}{2H_{G_i}} [T_{m_i} - T_{e_i}] \tag{5}$$

$$\dot{E}'_{qr_i} = -\frac{1}{T'_{o_i}} [E'_{qr_i} - (X_i - X'_i) i_{ds_i}] - s_i \omega_s E'_{dr_i} \tag{6}$$

$$\dot{E}'_{dr_i} = -\frac{1}{T'_{o_i}} [E'_{dr_i} + (X_i - X'_i) i_{qs_i}] + s_i \omega_s E'_{qr_i} \tag{7}$$

$$V_{ds_i} = R_{s_i} i_{ds_i} - X'_i i_{qs_i} + E'_{dr_i} \tag{8}$$

$$V_{qs_i} = R_{s_i} i_{ds_i} + X'_i i_{qs_i} + E'_{qr_i} \tag{9}$$

$$v_{t_i} = \sqrt{V_{ds_i}^2 + V_{qs_i}^2} \tag{10}$$

where $X'_i = X_{s_i} + X_{m_i} X_{r_i} / (X_{m_i} + X_{r_i})$, $X_i = X_{s_i} + X_{m_i}$, $T'_{o_i} = (L_{r_i} + L_{m_i})/R_{r_i}$ and $T_{e_i} = E_{dr_i} i_{ds_i} + E_{qr_i} i_{qs_i}$

The STATCOM is a shunt-connected device using power electronics to generate a three-phase voltage whose magnitude and phase angle can be adjusted rapidly. In this way, the STATCOM can inject capacitive or inductive current at the AC system bus. The traditional STATCOM has limited energy storage capability. Thus it is not possible to significantly impact both active and reactive power simultaneously with the traditional STATCOM. The fast active and reactive power support provided by an ESS (which may consist of a supercapacitor coupled to the STATCOM, for example) can significantly enhance the flexibility and control of transmission and distribution systems.

The main components of the STATCOM/ESS shown in Fig. 1 are a normal STATCOM and a supercapacitor-based ESS. A normal STATCOM is comprised of a coupling transformer, a voltage source inverter (VSC) and a DC link capacitor (usually electrolytic). The DC link capacitor provides voltage support for the VSC and the DC chopper. The ESS is comprised of a supercapacitor and a bi-directional DC–DC buck–boost converter to control the charging and discharging of the supercapacitor modules. The aim of these modules is to store energy in the supercapacitor and then deliver that energy to the grid via the DC link when required. The DC to DC converter

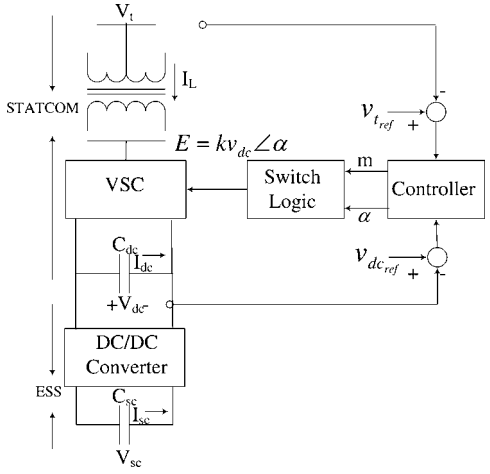

Fig. 1 *STATCOM/ESS control strategy*

operates in buck mode to recharge the supercapacitor, whereas boost mode transfers the stored energy to the DC link [20].

We can write equations for the STATCOM circuit as

$$\dot{v}_{\mathrm{dc}_l}(t) = -\frac{P_{s_l}}{C_l v_{\mathrm{dc}_l}} - \frac{v_{\mathrm{dc}_l}}{R_{c_l} C_l} \tag{11}$$

for $l = 1, 2, \ldots, m$, where m is the number of STATCOMs and P_{s_l} is the power supplied by the system to the STATCOM to charge the capacitor, given by

$$P_{s_l} = |E_l|^2 G_{ll} + \sum_{\substack{p=1 \\ p \neq l}}^{m} |E_l||E_p|[B_{lp} \sin \alpha_{pl} + G_{lp} \cos \alpha_{lp}] + \sum_{\substack{j=1 \\ j \neq l}}^{n} |E_l||E'_j|[B_{lj} \sin(\delta_j - \alpha_l) + G_{lj} \cos(\delta_j - \alpha_l)] \tag{12}$$

where G_{lp} and B_{lp} are the real and imaginary parts of the equivalent transfer impedances between the terminal buses of STATCOMs, l and p and G_{lj} and B_{lj} are between terminal buses of STATCOM, l and IG, j. The term E'_j denotes $E'_{\mathrm{d}rj}$, $E'_{\mathrm{q}rj}$ and E'_{qj}, and $\sin\alpha_{pl} = \sin(\alpha_p - \alpha_l)$. Also, the STATCOM terminal AC voltage is $E_l = k_l v_{\mathrm{dc}_l} \angle \alpha_l$, where α_l is the bus angle of the STATCOM in the reduced network, and $k_l = \sqrt{(3/8)} m_l$, where m_l is the modulation index. The terminal voltages of the STATCOMs are measured using transducers with first-order dynamic models of type

$$\dot{v}_{\mathrm{tm}_l} = -\frac{v_{\mathrm{tm}_l}}{T_{\mathrm{m}_l}} + K_{\mathrm{m}_l} v_{\mathrm{t}_l} \tag{13}$$

The dynamics of the supercapacitor is represented as

$$C_{\mathrm{sc}_i} \dot{v}_{\mathrm{dc}_r}(t) = -\frac{v_{\mathrm{sc}_r}}{R_{\mathrm{s}_r}} - \frac{v_{\mathrm{dc}_l}}{R_{\mathrm{s}_r}} \tag{14}$$

for $r = 1, 2, \ldots, p$, where p is the number of ESS.

The STATCOM/ESS controller is depicted in Fig. 1. The controller provides DC voltage and terminal voltage command to achieve the desired system response during the transient period. The controller converts the voltage command into pulse-width modulation (PWM) switching signals for the STATCOM/ESS. The designed multi-variable controller regulates the modulation gain m_i and firing angle (α_i). The firing angle α_i mainly affects the variation of the active power exchanged between the system whose input signal is the error signal between the measured DC voltage V_{dc} and the specified power reference ($V_{\mathrm{dc}_r\mathrm{ef}}$). Therefore the function of the active power control is to meet the active power demand of the system during transients. The other output of the controller is the duty cycle ratio m_i which mainly regulates the magnitude of the STATCOM's output voltage and therefore the system voltage.

4 Test system and control task

One-line diagram of the New England system [21] is shown in Fig. 2. This system is modified by replacing four conventional generators at buses 31–34 by four wind farms

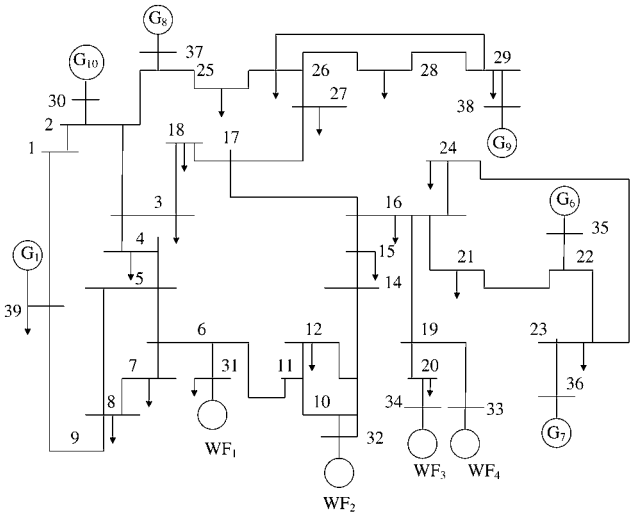

Fig. 2 *Ten machine 39 bus study system*

and used as the test system in this paper. The modified system network consists of six thermal power plants and four wind farms. The conventional generation, wind generation and the total load in this system are 3760.48, 2432.93 and 6150.5 MW, respectively. We used aggregated wind generator [22] and synchronous generator models [23] for controller design.

Two 150 kVA 2-level VSC-based STATCOM/ESS (95 F, 19 kJ) are connected to the system at buses 32 and 34 through shunt coupling transformers at 110 kV to regulate their respective terminal bus voltages at the point of common coupling (PCC). The most effective locations and best feedback signals for the STATCOM/ESS and the power system stabilisers (PSSs) are found by the method of comparing the residues, which are the products of modal controllability and observability gramians [24]. The modal controllability indicates the degree of influence of the given input to the mode in question. The modal observability is a measure of the modal information contained in a feedback signal. They are independent and hence can be computed separately. Buses 36 and 39 are the best locations for the PSSs. The selection of the STATCOM/ESSs and the PSSs locations and the best feedback signal are made by a comparison of the residues at all the locations.

The eigenvalue analysis of the original system (before replacing the conventional generation by wind farms) shows that it has a dominant mode at $-0.0131 \pm$ j0.711 with a damping ratio of 0.019. The modified system has three critical modes and their values with the most significant normalised participation vectors are shown in Table 1. The mode $-0.062 \pm$ j2.21 is an electromechanical mode with a damping ratio of 0.028. The other two unstable modes with eigenvalues 0.018 and 0.14 are monotonic modes associated with both the rotor electrical dynamics of IGs. These two monotonic modes are introduced because of the replacement of synchronous generation with IGs. In this paper, attention is directed to the design of robust control

Table 1 Critical modes and participation factors

Modes	Participation factors		
$-0.062 \pm$ j2.21	$\Delta\delta_6 = 1$	$\Delta\delta_1 = 0.7738$	$\Delta E_{\mathrm{dr}1} = 0.74$
0.018	$\Delta E'_{qr2} = 1$	$\Delta E'_{\mathrm{dr}2} = 0.52$	$\Delta s_2 = 0.49$
0.14	$\Delta E'_{qr4} = 1$	$\Delta E'_{\mathrm{dr}4} = 0.93$	$\Delta s_4 = 0.29$

doi: 10.1049/iet-gtd.2011.0537

for these unstable modes. From the participation vectors in Table 1, it is clear that the generators 6 and 1, and wind farms 1 and 2 contribute significantly to the dominant mode and controllers should be designed for both the synchronous and wind generators. This emphasises the need to design decentralised controllers.

The test system considered in this paper is divided into four sub-systems based on the coherent groups (generators swing together) of generating units: (i) wind farms 1 and 3, (ii) wind farms 2 and 4, (iii) G_6, G_9 and G_{10} and (iv) G_7, G_8 and G_1. One STATCOM/ESS controller each is a part of sub-systems 1 and 2, and the PSSs are parts of sub-systems 3 and 4. The PSSs are designed using the standard process given in [25]. For sub-systems 1 and 2, the state vector is $\Delta \boldsymbol{x}_i = [\Delta\omega_{m_i}, \Delta\omega_{G_i}, \Delta\gamma_i, \Delta s_i, \Delta E'_{\mathrm{dr}_i}, \Delta E'_{\mathrm{qr}_i}, \Delta v_{\mathrm{dc}i}, \Delta v_{\mathrm{tm}_i}, \Delta v_{\mathrm{sc}_i}]$, $i = 1, 2$. For STATCOM/ESS controllers, the control input $u_i = \begin{bmatrix} \Delta m_i & \Delta\alpha_i \end{bmatrix}^{\mathrm{T}}$, $y_i = \begin{bmatrix} \Delta v_{\mathrm{t}_i} & \Delta v_{\mathrm{dc}_i} \end{bmatrix}^{\mathrm{T}}$, and for (PSSs), $u_i = \Delta V_{\mathrm{s}_i}$ and $y_i = \Delta\omega_i$, where V_{s_i} is the PSS output signal and ω_i is the rotor speed of the synchronous generator.

5 Problem formulation

A linearised model of the power system is usually obtained by expanding the equations, around an equilibrium point, in a Taylor series and retaining only the linear terms. In this paper, in the design of the linear controller, the Cauchy remainder is incorporated as an uncertain term thus quantifying the deviations from the equilibrium point.

The reformulation proposed in this paper using Cauchy remainder allows us to represent the non-linear large scale power system S comprising n sub-systems S_i of the following form

$$S_i: \Delta\dot{x}_i = \boldsymbol{A}_i\Delta\boldsymbol{x}_i + \boldsymbol{B}_i\Delta\boldsymbol{u}_i + \boldsymbol{E}_i\boldsymbol{\xi}_i + \boldsymbol{L}_i r_i \tag{15}$$

$$z_i = \boldsymbol{C}_i\Delta\boldsymbol{x}_i + \boldsymbol{D}_i\Delta\boldsymbol{u}_i \tag{16}$$

$$\zeta_i = \boldsymbol{H}_i\Delta\boldsymbol{x}_i + \boldsymbol{G}_i\Delta\boldsymbol{u}_i \tag{17}$$

$$y_i = \boldsymbol{C}_{yi}\Delta\boldsymbol{x}_i + \boldsymbol{D}_{yi}\boldsymbol{\xi}_i \tag{18}$$

where $\Delta\boldsymbol{x}_i$ is the state vector, Δu_i is the control input, y_i is the measured output, z_i is the controlled output, ξ_i is known as the uncertainty input, ζ_i is known as the uncertainty output and r_i describes the effect of other sub-systems $S_1, \ldots, S_{i-1}, S_{i+1}, \ldots, S_N$ on sub-system S_i.

The procedure for obtaining the matrices in (15)–(18) and the bounding uncertainty is described in the rest of this section for the wind generator sub-system (sub-systems 1 and 2). The process is similar for the other sub-systems. Let (x_{i_0}, u_{i_0}) be an arbitrary point, using the mean-value theorem, the sub-system (2)–(10) with a wind turbine and a generator can be rewritten as follows [26]

$$\dot{x}_i = f_i(x_{i_0}, u_{i_0}) + P_i(x_i - x_{i0}) + Q_i(u_i - u_{i_0}) + \sum_{\substack{j=1 \\ j\neq i}}^{n} N_i(x_j - x_{j_0}) \tag{19}$$

where the Cauchy remainder terms are

$$\boldsymbol{P}_i = \begin{bmatrix} \left.\dfrac{\partial f_{i1}}{\partial x_i}\right|_{\substack{x_i=x_i^{*1}\\ u_i=u_i^{*1}}} \\ \vdots \\ \left.\dfrac{\partial f_{i9}}{\partial x_i}\right|_{\substack{x_i=x_i^{*9}\\ u_i=u_i^{*9}}} \end{bmatrix}, \quad \boldsymbol{Q}_i = \begin{bmatrix} \left.\dfrac{\partial f_{i1}}{\partial u_i}\right|_{\substack{x_i=x_i^{*1}\\ u_i=u_i^{*1}}} \\ \vdots \\ \left.\dfrac{\partial f_{i9}}{\partial u_i}\right|_{\substack{x_i=x_i^{*9}\\ u_i=u_i^{*9}}} \end{bmatrix},$$

$$\boldsymbol{N}_i = \sum_{\substack{j=1 \\ j\neq i}}^{n} \begin{bmatrix} \left.\dfrac{\partial f_{i1}}{\partial x_j}\right|_{\substack{x_i=x_i^{*1}\\ u_i=u_i^{*1}}} \\ \vdots \\ \left.\dfrac{\partial f_{i9}}{\partial x_j}\right|_{\substack{x_i=x_i^{*9}\\ x_i=u_i^{*9}}} \end{bmatrix}$$

Here $\boldsymbol{x}_i$ is a 1×9 column vector, $\boldsymbol{f}_i = [f_{i1}, \ldots, f_{i9}]^{\mathrm{T}}$ is also a 1×9 column vector made up of the right-hand-side of (2)–(10); (x_i^{*p}, u_i^{*p}), $p = 1, \ldots, 9$, denote points lying on the line segment connecting points (x_i, u_i) and (x_{i_0}, u_{i_0}). Equation (19) is an exact reformulation of the system in which the first term is linear and the rest of the terms are Cauchy remainders. The Cauchy remainder term can also be linear, but it has to be evaluated not at the system equilibrium point but on a point lying on the segment joining the equilibrium point and the current operating point.

It should be noted that the exact values of x_i^{*p} and u_i^{*p} are not available, and because of this, instead of the exact expressions for P_i, Q_i and N_i in system (19), their bounds, obtained numerically, are used in the control design.

Letting (x_{i0}, u_{i0}) be an equilibrium point and defining $\Delta x_i \triangleq x_i - x_{i0}$ and $\Delta u_i \triangleq u_i - u_{i0}$, it is possible to rewrite (19) as follows

$$\begin{aligned} \Delta\dot{x}_i &= \dot{x}_i - \dot{x}_{i0} \\ &= \boldsymbol{P}_i(x_i - x_{i0}) + \boldsymbol{Q}_i(u_i - u_{i0}) + N_i(x_j - x_{j0}) \\ &= \boldsymbol{A}_i\Delta x_i + (\boldsymbol{P}_i - \boldsymbol{A}_i)\Delta x_i + (\boldsymbol{Q}_i - \boldsymbol{B}_i)\Delta u_i + N_i\Delta x_j + \boldsymbol{B}_i\Delta u_i \end{aligned} \tag{20}$$

where $\boldsymbol{A}_i = \left.\dfrac{\partial f_i}{\partial x_i}\right|_{\substack{x_i=x_{i0}\\ u_i=u_{i0}}}$ and $\boldsymbol{B}_i = \left.\dfrac{\partial f_i}{\partial u_i}\right|_{\substack{x_i=x_{i0}\\ u_i=u_{i0}}}$ are the Jacobian matrices evaluated about the point $\{x_{i0}, u_{i0}\}$. It is important to note that both $\boldsymbol{A}_i$ and $\boldsymbol{B}_i$ are known matrices (Jacobians evaluated at the equilibrium point), while P_i and Q_i are unknown, because they depend on the x^{*p} and u^{*p}. Therefore we use a formulation with bounded uncertainties to account for the terms in which these unknown matrices appear.

The system (20) is of the form which allows for an application of the minimax control design technique [27]. To apply this technique, we rewrite system (20) in terms of the block diagram shown in Fig. 3.

Let

$$(\boldsymbol{P}_i - \boldsymbol{A}_i)\Delta x_i + (\boldsymbol{Q}_i - \boldsymbol{B}_i)\Delta u_i = E_i\xi_i \tag{21}$$

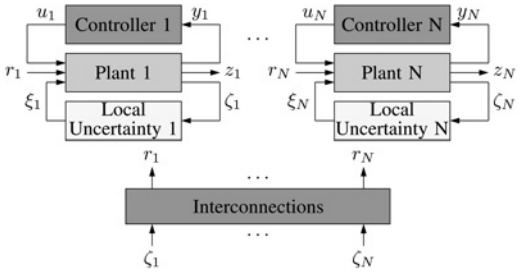

Fig. 3 *Block diagram of the uncertain system*

where

$$E_i = \mathrm{diag}\left(\frac{1}{2H_{m_i}}, \frac{1}{2H_{G_i}}, 0, \frac{1}{2H_{G_i}}, \frac{X_i - X_i'}{T_{o_i}'}, \frac{X_i - X_i'}{T_{o_i}'}, \frac{1}{\boldsymbol{C}_i}, T_{m_i}, 0\right)$$
$$\xi_i = \tilde{\phi}_i(\tilde{H}_i \Delta x_i) + \tilde{\boldsymbol{\psi}}_i(\tilde{G}_i \Delta u_i), \quad N_i \Delta x_j = L_i r_i \tag{22}$$

where $r_i = \sum_{\substack{j=1 \\ j \neq i}}^{n} \tilde{\Xi}_i \zeta_j$ and

$$\boldsymbol{H}_i = \sqrt{\Gamma_i}\begin{bmatrix} 0 & 0 & 0 & 1 & 0 & 0 & 0 & 0 & 0 \\ 0 & 0 & 0 & 0 & 1 & 0 & 0 & 0 & 0 \\ 0 & 0 & 0 & 0 & 0 & 1 & 0 & 0 & 0 \\ 0 & 0 & 0 & 0 & 0 & 0 & 1 & 0 & 0 \end{bmatrix}, \quad \boldsymbol{G}_i = \begin{bmatrix} 1 & 1 \\ 1 & 1 \\ 1 & 1 \\ 1 & 1 \end{bmatrix} \tag{23}$$

and $\boldsymbol{L}_i$ is a 9×9 identity matrix.

Non-linear functions $\tilde{\boldsymbol{\phi}}_i$ and $\tilde{\boldsymbol{\psi}}_i$ are obtained from the Jacobian matrices $\boldsymbol{P}_i$, $\boldsymbol{A}_i$, $\boldsymbol{Q}_i$ and $\boldsymbol{B}_i$. It is difficult to represent these matrices symbolically, but it is straightforward to evaluate them numerically at a given point and this is what we need to do to calculate the bounds on $\tilde{\boldsymbol{\phi}}_i$ and $\tilde{\boldsymbol{\psi}}_i$ over the region of interest. To obtain an idea of the form of the expressions, we give here a few sample expressions. Let $\tilde{\boldsymbol{\phi}}_i = [\tilde{\phi}_{i1}, \ldots, \tilde{\phi}_{i9}]^{\mathrm{T}}$, where

$$\tilde{\phi}_{i1} = \begin{bmatrix} 0 & 0 & 0 & 0 \end{bmatrix},$$
$$\tilde{\phi}_{i2} = \begin{bmatrix} x_{11} \\ x_{12} \\ x_{13} \\ x_{14} \\ x_{15} \\ x_{16} \end{bmatrix}^{\mathrm{T}} \begin{bmatrix} 0 & y_{12} & y_{13} & 0 \\ 0 & y_{22} & y_{23} & 0 \\ 0 & y_{32} & y_{33} & 0 \\ 0 & y_{42} & y_{43} & 0 \\ 0 & y_{52} & y_{53} & y_{54} \\ 0 & y_{62} & y_{63} & y_{64} \end{bmatrix} \tag{24}$$

where

$$x_{11} = \cos\delta_{ji}^* - \cos\delta_{ji0}, \quad x_{12} = \sin\delta_{ji}^* - \sin\delta_{ji0},$$
$$x_{13} = \cos(\delta_{m_k}^* - \delta_i^*) - \cos(\delta_{m_{k0}} - \delta_{i0}),$$
$$x_{14} = \sin(\delta_{m_k}^* - \delta_i^*) + \sin(\delta_{m_{k0}} - \delta_{i0}),$$
$$y_{12} = \sum_{j=1}^{n}(E_{\mathrm{dr}_j}'^* - E_{\mathrm{dr}_{j0}}')G_{ij} + \sum_{j=1}^{n}(E_{qr_j}'^* - E_{qr_{j0}}')\boldsymbol{B}_{ij},$$
$$y_{22} = -\sum_{j=1}^{n}(E_{\mathrm{dr}_j}'^* - E_{\mathrm{dr}_{j0}}')\boldsymbol{B}_{ij} + \sum_{j=1}^{n}(E_{qr_j}'^* - E_{qr_{j0}}')G_{ij},$$
$$y_{32} = \sum_{k=1}^{n}(E_{q_k}'^* - E_{q_{k0}}')\boldsymbol{B}_{ik},$$
$$x_{15} = \cos(\alpha_l^* - \delta_i^*) - \cos(\alpha_{l0} - \delta_{i0}),$$
$$y_{42} = \sum_{k=1}^{n}(E_{q_k}'^* - E_{q_{k0}}')G_{ik},$$
$$x_{16} = \sin(\alpha_l^* - \delta_i^*) - \sin(\delta_{l0} - \delta_{i0}),$$
$$y_{52} = -\sum_{l=1}^{n} k_l(v_{dc_l}^{*'} - v_{dc_{l0}})\boldsymbol{B}_{il},$$
$$y_{62} = \sum_{l=1}^{n} k_l(v_{dc_l}^{*'} - v_{dc_{l0}})G_{il}, \quad y_{13} = \sum_{j=1}^{n}(E_{\mathrm{dr}_j}'^* - E_{\mathrm{dr}_{j0}}')\boldsymbol{B}_{ij} + \sum_{j=1}^{n}(E_{qr_j}'^* - E_{qr_{j0}}')G_{ij},$$
$$y_{23} = -\sum_{j=1}^{n}(E_{\mathrm{dr}_j}'^* - E_{\mathrm{dr}_{j0}}')G_{ij} - \sum_{j=1}^{n}(E_{qr_j}'^* - E_{qr_{j0}}')\boldsymbol{B}_{ij},$$
$$y_{33} = \sum_{k=1}^{n}(E_{q_k}'^* - E_{q_{k0}}')G_{ik},$$
$$y_{43} = -\sum_{k=1}^{n}(E_{q_k}'^* - E_{q_{k0}}')\boldsymbol{B}_{ik},$$
$$y_{53} = \sum_{l=1}^{n}\kappa_l(v_{dc_l}^{*'} - v_{dc_{l0}})G_{il},$$
$$y_{63} = \sum_{l=1}^{n}\kappa_l(v_{dc_l}^{*'} - v_{dc_{l0}})\boldsymbol{B}_{il}, \quad y_{54} = \sum_{l=1}^{n}\kappa_l(E_{\mathrm{dr}_i}'^* - E_{\mathrm{dr}_{i0}}')\boldsymbol{B}_{il} + \sum_{l=1}^{n}(E_{qr_i}'^* - E_{qr_{i0}}')G_{il},$$
$$y_{64} = \sum_{l=1}^{n}\kappa_l(E_{\mathrm{dr}_i}'^* - E_{\mathrm{dr}_{i0}}')G_{il} + \sum_{l=1}^{n}(E_{\mathrm{qr}_i}'^* - E_{\mathrm{qr}_{i0}}')G_{il}$$

Given that uncertainties in this paper derive from non-linearities, the terms that have linear relations with the state variables will be represented by zeros in the corresponding matrices. The rest of the expressions of $\tilde{\phi}_i$, $\tilde{\psi}_i$ and $\tilde{\Xi}_i$ can be determined in a similar way as in [15].

The system (20) now can be rewritten as

$$\Delta\dot{x}_i = \boldsymbol{A}_i \Delta x_i + \boldsymbol{B}_i \Delta u_i + E_i \xi_i + L_i r_i \tag{25}$$

Next, we introduce a scaling parameter Γ_i such that the product terms $\tilde{\phi}_i\tilde{H}_i$ and $\tilde{\psi}_i\tilde{G}_i$, are factored into two parts. We define

$$H_i = \sqrt{\Gamma_i}\tilde{H}_i, \quad \text{and} \quad G_i = \sqrt{\Gamma_i}\tilde{G}_i \tag{26}$$

from this it can be seen that Γ_i is a scaling factor that affects the magnitude of the uncertain output ζ_i. Scaling permits us to

doi: 10.1049/iet-gtd.2011.0537

obtain less conservative results. We write

$$\boldsymbol{\phi}_i = \frac{1}{\sqrt{\Gamma_i}}[\,\tilde{\phi}_i \quad \tilde{\psi}_i\,] \quad \text{and} \quad \Xi_i = \frac{1}{\sqrt{\Gamma_i}}\tilde{\Xi}_i \tag{27}$$

Finally the value of Γ_i is chosen such that

$$\| \phi_i \|^2 \leq 1 \quad \text{and} \quad \| \Xi_i \|^2 \leq 1 \tag{28}$$

From (22) and (28) we have

$$\| \xi_i \|^2 \leq \Gamma_i \| \tilde{H}_i \Delta x_i + \tilde{G}_i \Delta u_i \|^2 \tag{29}$$

We also define $\zeta_i = \tilde{H}_i \Delta x_i + \tilde{G}_i \Delta u_i$, and from this, we recover the norm bound constraints [28]

$$\| \xi_i \|^2 \leq \| \zeta_i \|^2 \quad \text{and} \quad \| r_i \|^2 \leq \sum_{j \neq i} \| \zeta_j \|^2 \tag{30}$$

The bounds given in (30) can be used with the linear quadratic (LQ) output-feedback control design method to obtain a controller for the underlying non-linear system. Robustness properties of the LQ output controller ensure that this controller stabilises the non-linear system (15)–(18) for all instances of linearisation errors. The relationship between the maximum size of ϕ_i and the elements in (24) is complicated and not easy to see. Two observations are useful: (a) larger values of elements in $\boldsymbol{G}$ and $\boldsymbol{B}$ matrices lead to larger size of ϕ_i, and (b) the maximum value of ϕ_i is not achieved at the corner points of the polytope but at interior points.

Equations (15)–(18) provide a new representation of the power system model with a linear part, and another part with higher order terms. For this controller design, we consider

$$\boldsymbol{C}_i = [0, 0, 0, 1, 0, 0, 0, 0, 0]^{\mathrm{T}}, \quad \boldsymbol{D}_i = 10^{-4}[1, 1]^{\mathrm{T}} \tag{31}$$

$$\boldsymbol{C}_{yi} = [0, 0, 0, 0, 0, 0, 0, 1, 0; 0, 0, 0, 0, 0, 0, 0, 0, 1]^{\mathrm{T}} \tag{32}$$

$$\boldsymbol{D}_{yi} = 10^{-4}[0, 0, 0, 1, 1, 1, 1, 0, 0; 0, 0, 0, 1, 1, 1, 1, 0, 0]^{\mathrm{T}} \tag{33}$$

The new formulation presented in this section is used with the LQ output-feedback control theory to design decentralised controllers for the non-linear power system.

6 Decentralised control design using rank constrained LMIs

In this paper, a decentralised LQ output-feedback control has been designed using LMI techniques [28, 29]. The control design procedure given in [28] has been modified here for a single mode.

The robust control design methodology developed in [28] makes use of integral quadratic constraints (IQC) to characterise the magnitude of uncertain perturbations and interconnection between sub-systems

$$E\int_0^{t_l} (\| \zeta_i(t) \|^2 - \| \xi_i(t) \|^2)\, \mathrm{d}t > -x_{i0}^{\mathrm{T}} M_i x_{i0} \tag{34}$$

$$E\int_0^{t_l} \left(\sum_{n=1, n\neq i}^{N} \| \zeta_n(t) \|^2 - \| r_i(t) \|^2 \right) \mathrm{d}t > -x_{i0}^{\mathrm{T}} \bar{M}_i x_{i0} \tag{35}$$

where $M_i = M_i^{\mathrm{T}} > 0$, $\bar{M}_i = \bar{M}_i^{\mathrm{T}} > 0$, $\{t_l\}_{l=1}^{\infty}$, $t_l \to +\infty$, is a sequence of time instants and E is the expectation operator. It is obvious that the constraints (30) can be rewritten in the form of (34) and (35) with arbitrarily chosen small $x_{i0}^{\mathrm{T}} M_i x_{i0}$ and $x_{i0}^{\mathrm{T}} \bar{M}_i x_{i0}$.

This LQ technique minimises the following performance cost over all permissible IQCs

$$J_{\mathrm{wc}}(u) \triangleq \int_0^{\infty} \sum_{i=1}^{N} \| z_i(t) \|^2 \, \mathrm{d}t \tag{36}$$

In this paper, we consider norm bounded constraints, as in (30), instead of the more general IQCs. This means that the designed controllers are sub-optimal for norm bounded constraints. The control algorithm is to find the infimum of the following function over the set $\mathcal{T}$

$$J(\tau, \theta) = \sum_{i=1}^{N} x_{i0}^{\mathrm{T}} [\bar{X}_i + \tau_i M_i + \theta_i \bar{M}_i] x_{i0} \tag{37}$$

where $\mathcal{T} = \{\{\tau_i \theta_i\} \in R^{2N}, \tau_i > 0, \theta_i > 0\}$, $\boldsymbol{M}_i > 0$ and $\bar{M}_i > 0$ are two sets of symmetric matrices, and matrices $\bar{\boldsymbol{X}}_i$ and $\bar{\boldsymbol{Y}}_i$ are the solutions to the following pair of coupled generalised algebraic Riccati equations and algebraic Riccati inequalities [28]

$$\boldsymbol{A}_i^{\mathrm{T}} \bar{\boldsymbol{X}}_i + \bar{\boldsymbol{X}}_i \boldsymbol{A}_i + \bar{\boldsymbol{C}}_i^{\mathrm{T}} \bar{\boldsymbol{C}}_i - \bar{\boldsymbol{X}}_i [\boldsymbol{B}_i R_i^{-1} \boldsymbol{B}_i^{\mathrm{T}} - \bar{\boldsymbol{B}}_{2_i} \bar{\boldsymbol{B}}_{2_i}^{\mathrm{T}}] \bar{\boldsymbol{X}}_i = 0 \tag{38}$$

$$\boldsymbol{A}_i^{\mathrm{T}} \bar{\boldsymbol{Y}}_i + \bar{\boldsymbol{Y}}_i \boldsymbol{A}_i + \bar{\boldsymbol{Y}}_i \bar{\boldsymbol{B}}_{2_i} \bar{\boldsymbol{B}}_{2_i}^{\mathrm{T}} \bar{\boldsymbol{Y}}_i - [\boldsymbol{C}_{y_i}^{\mathrm{T}} W_i^{-1} \boldsymbol{C}_{y_i} - \bar{\boldsymbol{C}}_i^{\mathrm{T}} \bar{\boldsymbol{C}}_i] < 0 \tag{39}$$

where $R_i = \bar{\boldsymbol{D}}_i^{\mathrm{T}} \bar{\boldsymbol{D}}_i$, $W_i = \bar{\boldsymbol{D}}_{y_i} \bar{\boldsymbol{D}}_{y_i}^{\mathrm{T}}$, $\bar{\theta}_i = \sum_{n=1, n\neq i}^{N} \theta_n$,

$$\begin{aligned} \bar{\boldsymbol{C}}_i &= \begin{bmatrix} \boldsymbol{C}_i \\ (\tau_i + \bar{\theta}_i)^{1/2} H_i \end{bmatrix}, \quad \bar{\boldsymbol{D}}_i = \begin{bmatrix} \boldsymbol{D}_i \\ (\tau_i + \bar{\theta}_i)^{1/2} G_i \end{bmatrix} \\ \bar{B}_{2_i} &= \begin{bmatrix} \tau_i^{-1/2} E_i & \theta_i^{-1/2} L_i \end{bmatrix}, \quad \bar{\boldsymbol{D}}_{y_i} = \begin{bmatrix} \tau_i^{-1/2} \boldsymbol{D}_{y_i} & 0 \end{bmatrix} \end{aligned} \tag{40}$$

The controller u_i^* with the τ^*, θ^* is given by [28]

$$\begin{aligned} \dot{x}_{c_i} = {} & \{\boldsymbol{A}_i - [\boldsymbol{B}_i R^{-1} \boldsymbol{B}_i^{\mathrm{T}} - \bar{\boldsymbol{B}}_{2_i} \bar{\boldsymbol{B}}_{2_i}^{\mathrm{T}}] \bar{\boldsymbol{X}}_i\} x_{c_i} \\ & + [\bar{\boldsymbol{Y}}_i - \bar{\boldsymbol{X}}_i]^{-1} \boldsymbol{C}_{y_i}^{\mathrm{T}} W_i^{-1} [y_i - \boldsymbol{C}_{y_i} x_{c_i}] \end{aligned} \tag{41}$$

$$u_i^* = -R_i^{-1} \boldsymbol{B}_i^{\mathrm{T}} \bar{\boldsymbol{X}}_i x_{c_i} \tag{42}$$

The solutions are required to satisfy the following conditions: $\tau_i > 0$, $\theta_i > 0$, $\bar{\boldsymbol{X}}_i \geq 0$, $\bar{\boldsymbol{Y}}_i \geq 0$ and $\bar{\boldsymbol{Y}}_i > \bar{\boldsymbol{X}}_i$.

The controller u^* guarantees the following minimax property

$$J_{\text{wc}}(u^*) \leq J(\tau^*, \theta^*) = \inf_{\mathcal{T}} J(\tau, \theta) \tag{43}$$

The solution of the optimisation problem using the LMI technique is discussed in Section 11 (Appendix).

7 Control design algorithm

The controller, in this section, is designed for severe faults so it can, in principle, also ensure stability against other disturbances. From fault simulations we estimated the operating region Ω formed by corner points $[\bar{s}_i, \bar{E}'_{\text{dr}_i}, \bar{E}'_{\text{qr}_i}, \bar{\omega}_{m_i}, \bar{\omega}_{G_i}, \bar{\gamma}_i, \bar{v}_{\text{dc}_i}, \bar{v}_{\text{tm}_i}, \bar{v}_{\text{sc}_i}]^{\text{T}}$ and $[s_i, \underline{E}'_{\text{dr}_i}, \underline{E}'_{\text{qr}_i}, \underline{\omega}_{m_i}, \underline{\omega}_{G_i}, \underline{\gamma}_i, v_{\text{dc}_i}, v_{\text{tm}_i}, v_{\text{sc}_i}]^{\text{T}}$ centred at equilibrium point for severe faults with the values $\bar{s}_i - s_i = 2 \times 0.225$ pu, $\bar{E}'_{\text{dr}_i} - \underline{E}'_{\text{dr}_i} = 2 \times 0.242$ pu, $\bar{E}'_{\text{qr}_i} - \underline{E}'_{\text{qr}_i} = 2 \times 0.225$ pu, $\bar{\omega}_{m_i} - \underline{\omega}_{m_i} = 2 \times 0.395$ pu, $\bar{\omega}_{G_i} - \underline{\omega}_{G_i} = 2 \times 0.337$ pu, $\bar{\gamma}_i - \underline{\gamma}_i = 2 \times 25^\circ$, $\bar{v}_{\text{dc}_i} - \underline{v}_{\text{dc}_i} = 2 \times 0.334$ pu, $\bar{v}_{\text{tm}_i} - \underline{v}_{\text{tm}_i} = 2 \times 0.235$ pu, $\bar{v}_{\text{sc}_i} - \underline{v}_{\text{sc}_i} = 2 \times 0.248$ pu, $\bar{m}_i - \underline{m}_i = 2 \times 0.328$ and $\bar{\alpha}_i - \underline{\alpha}_i = 2 \times 28^\circ$, $i = 1, 2$. The design process is described in the following steps:

(i) From simulations, select coherent groups of generating units and represent them by equivalent models.
(ii) Perform modal analysis and determine the critical modes. Analyse the participation vectors for the critical modes and identify the states related to them.
(iii) From the simulations of the faulted system (undergoing a large perturbation during the LVRT transient), obtain the range in variations of all state variables and form a volume, Ω, with corner points given by $(x_{f_p} - x_{0_p})$ and $(x_{f_p} + x_{0_p})$, $p = 1, \ldots, 7$, where $2x_{f_p}$ is the largest variation in the pth state variable about its equilibrium value, x_{0_p}.
(iv) Obtain $\Gamma_i^* = \max_{x_i^{sp} \in \Omega_i} \{\Gamma_i : ||\phi_i||^2 < 1, ||\Xi_i||^2 < 1\}$, as given in (28). The process to obtain Γ_i^* involves obtaining the maximum value of $\tilde{\phi}_i$, $\tilde{\psi}_i$, and Ξ_i over the entire region of interest and then using (27) to choose Γ_i such that $\|\phi_i\|^2 < 1$ and $\|\Xi_i\|^2 < 1$.
(v) Check if there exists a feasible controller with $\Gamma_i = \Gamma_i^*$, that is scalars τ_i and θ_i exist such that there is a feasible solution to LMIs, as described in Section 11.
(vi) Compare the control region with the operating region required to provide the LVRT capability of wind generators.
(vii) If we obtain a feasible controller in the above step, increase the range of the operating region if step (vi) is not satisfied or, if we have arrived at the largest possible range then perform an optimal search over the scalar parameters τ_i and θ_i, to obtain the infimum in (6). If there is no feasible solution with the chosen $\Gamma_i = \Gamma_i^*$, reduce the range and go to step (iv).

For the given system, we are able to obtain feasible controllers with values of $\Gamma_1 = 0.968$ and $\Gamma_2 = 0.976$. The controller is stabilising for all variation of states in the polytope region Ω formed by corner points $[\bar{s}_i, \bar{E}'_{\text{dr}_i}, \bar{E}'_{\text{qr}_i}, \omega_{m_i}, \bar{\omega}_{G_i}, \bar{\gamma}_i, \bar{v}_{\text{dc}_i}, \bar{v}_{\text{tm}_i}, \bar{v}_{\text{sc}_i}]^{\text{T}}$ and $[s_i, \underline{E}'_{\text{dr}_i}, \underline{E}'_{\text{qr}_i}, \underline{\omega}_{m_i}, \underline{\omega}_{G_i}, \underline{\gamma}_i, v_{\text{dc}_i}, v_{\text{tm}_i}, v_{\text{sc}_i}]^{\text{T}}$ with the following values: $\bar{s}_i = s_{i0} + 0.243$ pu, $s_i = s_{i0} - 0.243$ pu, $\bar{E}'_{\text{dr}_i} = E'_{\text{dr}_{i0}} + 0.347$ pu, $\underline{E}'_{\text{dr}_i} = E'_{\text{dr}_{i0}} - 0.347$ pu, $\bar{E}'_{\text{qr}_i} = E'_{\text{qr}_{i0}} + 0.315$ pu, $\underline{E}'_{\text{qr}_i} = E'_{\text{qr}_{i0}} - 0.315$ pu, $\bar{\omega}_{m_i} = \omega_{m_{i0}} + 0.428$ pu, $\underline{\omega}_{m_i} = \omega_{m_{i0}} - 0.428$ pu, $\bar{\omega}_{G_i} = \omega_{G_{i0}} + 0.437$ pu, $\underline{\omega}_{G_i} = \omega_{G_{i0}} - 0.437$ pu, $\bar{\gamma}_i = \gamma_{i0} + 36^\circ$, $\underline{\gamma}_i = \gamma_{i0} - 36^\circ$, $\bar{v}_{\text{dc}_i} = v_{\text{dc}_{i0}} + 0.365$ pu, $\underline{v}_{\text{dc}_i} = v_{\text{dc}_{i0}} - 0.365$ pu, $\bar{v}_{\text{tm}_i} = v_{\text{tm}_{i0}} + 0.269$ pu, $\underline{v}_{\text{tm}_i} = v_{\text{tm}_{i0}} - 0.269$ pu, $\bar{v}_{\text{sc}_i} = v_{\text{sc}_{i0}} + 0.275$ pu, $\underline{v}_{\text{sc}_i} = v_{\text{sc}_{i0}} - 0.275$ pu, $\bar{m}_i = m_{i0} - 0.467$, $\underline{m}_i = m_{i0} - 0.467$, $\bar{\alpha}_i = \alpha_{i0} + 23^\circ$ and $\underline{\alpha}_i = \alpha_{i0} - 23^\circ$, $i = 1, 2$. This range of the variation of the state variables is larger than the range for several large disturbances as noted earlier in this sub-section. The above bound for $\phi(\zeta)$ is obtained at a point interior to the region, that is $s_i^* = 0.185$ pu, $E'^*_{\text{dr}_i} = 0.85$ pu, $E'^*_{\text{qr}_i} = 0.825$ pu, $\omega^*_{m_i} = 1.45$ pu, $\omega^*_{G_i} = 1.42$ pu, $\gamma_i^* = 25.5^\circ$, $v^*_{\text{dc}_i} = 0.86$ pu, $v^*_{\text{sc}_i} = 0.845$ pu, $m_i^* = 0.425$ pu and $\alpha_i^* = 22.5^\circ$, $i = 1, 2$. Although the designed controller is not globally stabilising yet we know that it is stabilising over a large operating region which covers most faulted system operation. From the two cross-sections of the polytope Ω shown in Fig. 6*a*, it can be seen that the region of controller operation is larger than the region of faulted system trajectories.

8 Controller performance evaluation

8.1 Enhancement of voltage and transient stability margins

The LVRT capability of a wind generator is expressed in this paper as voltage and transient stability margins. The voltage stability margin is defined as the difference between the operating voltage and the critical voltage. The transient stability margin is given as the difference between the speed after a specified fault duration and the critical speed (CS) of the generator. The CS is given by the intersection between the torque-speed curve for the specified system and the mechanical torque [30]. The critical voltage can be obtained from the P–V curves [31]. The stability analysis of a power system may consider the determination of its critical clearing time (CCT), for a given fault, in order to find the maximum value of the CCT for which the system is still stable. In this paper, the CCT is first estimated by using (44) and then an exact value is determined from simulations in which it is obtained by increasing the fault time interval until the system loses its stability [32].

$$t_{\text{c}} = \frac{1}{T_{\text{m}}} 2H_m(s_{\text{c}} - s_0) \tag{44}$$

where t_{c} is the CCT, s_{c} is the critical slip and s_0 is the slip at equilibration point of a generator.

A simulation study is performed to emulate the system in Fig. 2 with the purpose of evaluating the transient and voltage stability limits achievable with the proposed and PI-based STATCOM/ESS. The CCT and CS, as shown in Table 2, for a three-phase fault with 150 MVA STATCOMs and 95 F, 19 kJ supercapacitors are 0.165 s and 1.35 pu with the designed controller, compared with 0.140 s and 1.315 pu with a properly tuned PI controller [20]. In this case, the gain of the tuned (trial and error method) PI controller is obtained as $K_{\text{P}} = 0.28$ and $K_{\text{I}} = 20.45$. It can be concluded that an appropriate combination of active and reactive power control by STATCOM/ESS is an effective way of improving the stability and enhancing the fault ride-through capability of the relevant induction-generator-based wind turbines.

In order to evaluate the performance of the designed controller, in the face of system non-linearity and operating conditions, detailed simulations are performed for a symmetrical 3-phase fault at bus 11 which is subsequently cleared after 150 ms. Figs. 4*a* and *b* show the speed response and terminal voltages, respectively, of the wind farm WF_1 with the conventional PI controller and the

doi: 10.1049/iet-gtd.2011.0537

Table 2 Performance comparison: (a) proposed controller and (b) PI-based STATCOM/ESS

STATCOM/ESS	(a) Proposed controller			(b) PI control		
	CS	CCT	Critical voltage	CS	CCT	Critical voltage
150 MVA/95 F	1.35 pu	0.165 s	0.605 pu	1.315 pu	0.140 s	0.625 pu

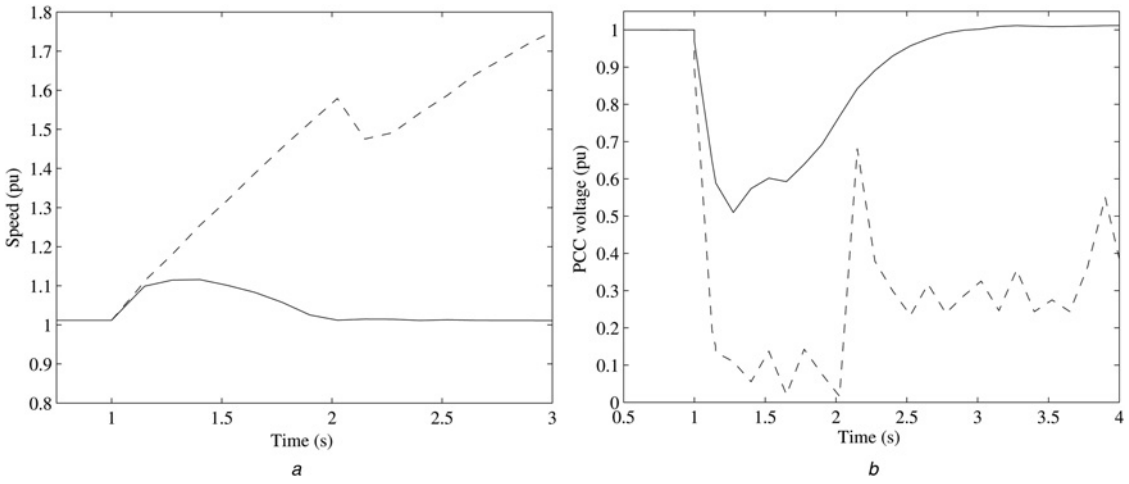

Fig. 4 *Speed and terminal voltage for three-phase fault at bus 11 (Solid line designed and dash line PI-based STATCOM/ESS)*
a Speed response
b Terminal voltage

proposed STATCOM/ESS controller. During the fault, the wind generator accelerates, since it is no longer able to generate enough electromagnetic torque to balance the mechanical torque coming from the wind which is obviously unaffected by the grid fault. When the fault is cleared, the generator speed with the proposed control is about 1.15 pu whereas that with the PI control is 1.6 pu. The reclosing time, speed and voltage using the PI controller is greater than the corresponding CCT, CS and critical voltage with the proposed controller. With the PI controller it can be seen that the terminal voltage cannot be restored and the IG continues to accelerate until the system loses stability.

8.2 Comparisons with standard LVRT requirements

Interconnection standards vary from country to country and among individual provinces or states, depending on local grid characteristics and utility specific requirements. In this research work, the standard jointly recommended by the North American Electric Reliability Council (NAERC) and the American Wind Energy Association (AWEA) [33] is used. This standard demands that if the voltage remains at a level greater than 15% of the nominal voltage for a period that does not exceed 0.625 s, the plant must stay online. Ireland also follows a similar standard [34]. Although this standard is followed in this research work, the designed controller fulfils the other grid codes as well. Fig. 5 shows the terminal voltage of the wind farm WF_2 with the proposed STATCOM/ESS controller with zero voltage for the duration of 300 ms from which it is clear that the proposed control can meet the standard requirement of the LVRT capability. The reason for providing stability during the LVRT transient is clear from Figs. 6*a* and *b*, which show that the control region provided by the designed controller is larger than the area required for the LVRT. A similar comparison holds true for other state variables.

8.3 Impact of adding supercapacitors

To test the effects of adding supercapacitors, a simulation is performed with (i) STATCOM/ESS and (ii) STATCOM only. A three-phase fault is applied at the middle of the line 16–17 at 1 s and the fault is cleared after 140 ms by opening the line 16–17. This line is again restored after 150 ms. Figs. 7*a* and *b* show the voltage and real power output of WF_2 from which, it is clear that although the addition of supercapacitor does not produce a significant difference in terminal voltage response, however, it damps

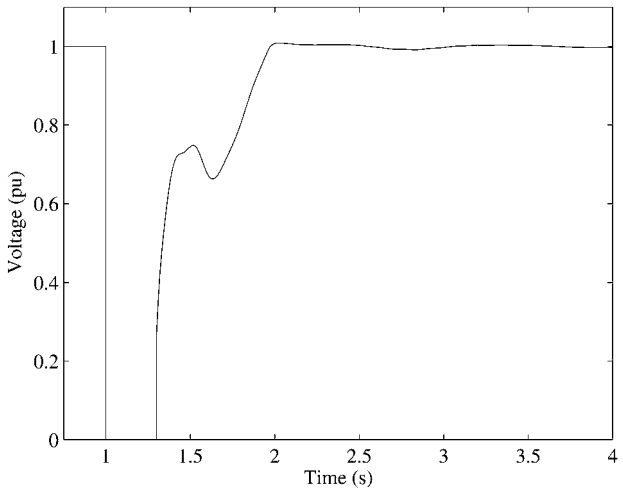

Fig. 5 *Terminal voltage with zero-voltage for 300 ms*

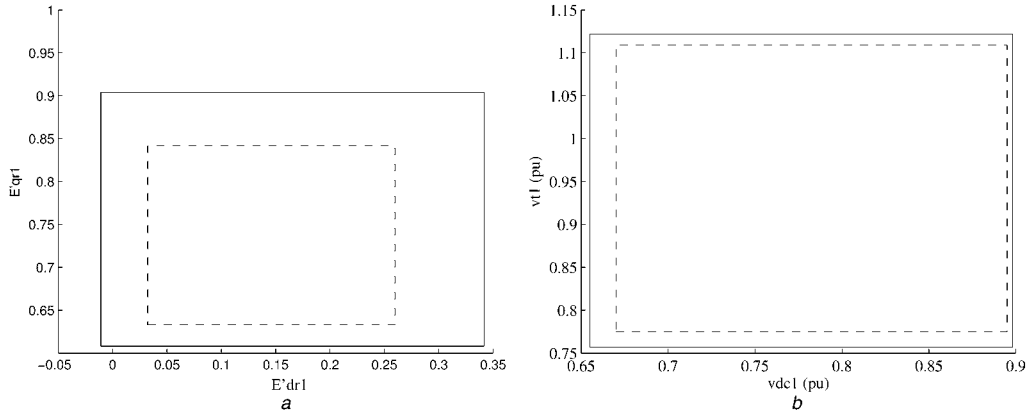

Fig. 6 *Operating and control region (solid line control region and dashed line operating region during LVRT transient)*

a *d*-axis and *q*-axis transient emf polytope section
b Capacitor voltage and terminal voltage polytope section

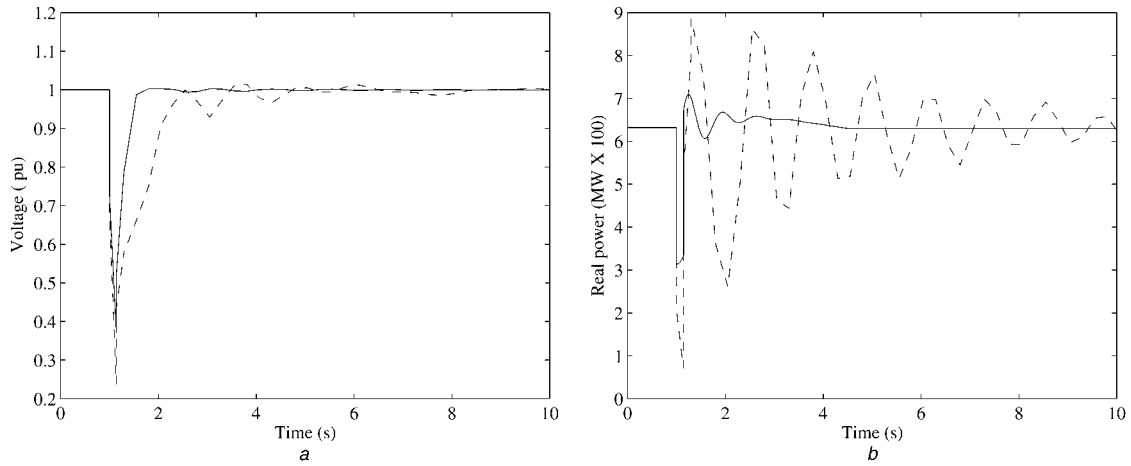

Fig. 7 *Voltage and real power output for a three-phase fault on line 16–17 (solid line designed STATCOM/ESS controller and dash line STATCOM without ESS controller)*

a Voltage response
b Real power output

the oscillation in output power quickly. The active power is controlled using energy storage-type supercapacitor and this is effective in enhancing the transient stability of the rest of the system.

9 Conclusions

In this paper, a new robust decentralised STATCOM/ESS control has been proposed to enhance the LVRT capability of fixed-speed wind turbines. A systematic procedure to design the controller has been discussed. The designed controller guarantees stability if the system post-fault operating point is in the region for which the controller is designed. A ten-machine power system has been used to evaluate the performance of the designed controller. Simulation results show that despite the non-linear interconnections between different types of generators and significant operating condition variations following fault, the proposed controller can greatly enhance the transient and voltage stability as well as LVRT capability of wind turbines. The future perspective of this work is to design reduced order controllers for distributed systems.

10 References

1 Leon, J.A.D.D., Taylor, C.W.: 'Understanding and solving short term voltage instability'. Proc. IEEE Power Engineering Society Summer Meeting, Illinois, Chicago, July 2002, pp. 745–752
2 De Alegría, I.M., Andreu, J., Martin, J.L., Ibañez, P., Villate, J.L., Camblong, H.: 'Connection requirements for wind farms: a survey on technical requirements and regulation', *Renew. Sustain. Energy Rev.*, 2007, **11**, (8), pp. 1858–1872
3 Suul, J.A., Molinas, M., Undeland, T.: 'STATCOM-based indirect torque control of induction machines during voltage recovery after grid faults', *IEEE Trans. Power Electron.*, 2010, **25**, (5), pp. 1240–1250
4 El-Moursi, M.S., Bak-Jensen, B., Abdel-Rahman, M.H.: 'Novel STATCOM controller for mitigating SSR and damping power system oscillations in a series compensated wind park', *IEEE Trans. Power Electron.*, 2010, **25**, (2), pp. 429–441
5 Rahimi, M., Parniani, M.: 'Efficient control scheme of wind turbines with doubly fed induction generators for low-voltage ride-through capability enhancement', *IET Renew. Power Gener.*, 2010, **4**, (3), pp. 242–252
6 Singh, B., Kasal, G.K.: 'Voltage and frequency controller for a three-phase four-wire autonomous wind energy conversion system', *IEEE Trans. Energy Convers.*, 2008, **23**, (2), pp. 509–518
7 Kamwa, I., Grondin, R., Hebert, Y.: 'Wide-area measurement based stabilizing control of large power systems-a decentralized/hierarchical approach', *IEEE Trans. Power Syst.*, 2001, **16**, (1), pp. 136–153
8 Hossain, M.J., Pota, H.R., Kumble, C.: 'Decentralized robust static synchronous compensator control for wind farms to augment dynamic transfer capability', *J. Renew. Sustain. Energy*, 2010, **2**, (2), pp. 022701(1)–022701(20)

doi: 10.1049/iet-gtd.2011.0537

9 Siljak, D.D., Zecevic, A.I., Neskovic, G.: 'Robust decentralized exciter control with linear feedback', *IEEE Trans. Power Syst.*, 2004, **19**, (2), pp. 1096–1103
10 Guo, Y., Hill, D.J., Wang, Y.: 'Nonlinear decentralized control of large-scale power systems', *Automatica*, 2000, **36**, (9), pp. 1275–1289
11 Siljak, D.D., Stipanovic, D.M., Zecevic, A.I.: 'Robust decentralized turbine/governor control using linear matrix inequalities', *IEEE Trans. Power Syst.*, 2002, **17**, (3), pp. 715–722
12 Siljak, D.D., Zecevic, A.I.: 'Control of large-scale systems: beyond decentralized feedback', *Annu. Rev. Control*, 2005, **29**, (2), pp. 169–179
13 Hossain, M.J., Pota, H.R., Ugrinovskii, V., Ramos, R.A.: 'Simultaneous STATCOM and pitch angle control for improved LVRT capability of fixed-speed wind turbines', *IEEE Trans. Sustain. Energy*, 2010, **1**, (3), pp. 142–151
14 Guo, Y., Hill, D.J., Wang, Y.: 'Global transient stability and voltage regulation for power systems', *IEEE Trans. Power Syst.*, 2001, **16**, (4), pp. 678–688
15 Hossain, M.J., Pota, H.R., Ugrinovskii, V., Ramos, R.A.: 'Excitation control for large disturbances in power systems with dynamic loads'. Proc. IEEE Power and Energy Society General Meeting, Calgary, Canada, July 2009, pp. 1–8
16 Hossain, M.J., Pota, H.R., Ugrinovskii, V.: 'Short and long-term dynamic voltage instability'. Proc. 17th IFAC World Congress, Seoul, Korea, July 2008, pp. 9392–9397
17 Ackermann, T.: 'Wind power in power systems' (John Wiley and Sons Ltd, England, 2005)
18 Abdin, E.S., Xu, W.: 'Control design and dynamic performance analysis of a wind turbine-induction generator unit', *IEEE Trans. Energy Convers.*, 2000, **15**, (1), pp. 91–96
19 Nandigam, K., Chowdhury, B.H.: 'Power flow and stability models for induction generators used in wind turbines'. Proc. IEEE Power Eng. Society General Meeting, June 2004, pp. 2012–2016
20 Srithorn, P., Sumner, M., Yao, L., Parashar, R.: 'A STATCOM with supercapacitors for enhanced power system stability'. Proc. 4th IET Conf. on Power Electronics, Machines and Drives, London, April 2008, pp. 96–100
21 Hiskens, I.A.: , Power system test cases. Available at: http://psdyn.ece.wisc.edu/IEEEbenchmarks/, accessed 1999
22 Fernandez, L., Garcia, C., Saenz, J., Jurado, F.: 'Equivalent models of wind farms by using aggregated wind turbines and equivalent winds', *Energy Convers. Manage.*, 2009, **50**, (3), pp. 691–704
23 Germond, A.J., Podmore, R.: 'Dynamic aggregation of generating unit models', *IEEE Trans. Power Appar. Syst.*, 1978, **97**, (4), pp. 1060–1069
24 Pal, B.C., Coonick, A.H., Macdonald, D.C.: 'Robust damping controller design in power systems with superconducting magnetic energy storage devices', *IEEE Trans. Power Syst.*, 2000, **15**, (1), pp. 320–325
25 Werner, H., Korba, P., Yang, T.C.: 'Robust tuning of power system stabilizers using LMI-techniques', *IEEE Trans. Control Syst. Technol.*, 2003, **11**, (2), pp. 147–152
26 Khalil, H.K.: 'Nonlinear systems' (Macmillan, Prentice-Hall, New York, 1992)
27 Petersen, I.R., Ugrinovskii, V.A., Savkin, A.V.: 'Robust control design using H_∞ methods' (Springer, London, 2000)
28 Li, L., Ugrinovskii, V.A., Orsi, R.: 'Decentralized robust control of uncertain Markov jump parameter systems via output feedback', *Automatica*, 2007, **43**, (11), pp. 1932–1944
29 Li, L., Petersen, I.R.: 'A rank constrained LMI algorithm for the robust H_∞ control of an uncertain system via a stable output feedback controller'. Proc. 46th IEEE Conf. on Decision and Control, New Orleans, Louisiana, USA, December 2007, pp. 5423–5428
30 Akhmatov, V., Knudsen, H., Bruntt, M., Nielsen, A., Pedersen, J.K., Poulsen, N.K.: 'A dynamic stability limit of grid-connected induction generator'. Proc. Int. Conf. on Power and Energy Systems, September 2000, pp. 235–244
31 Cutsem, T.V., Vournas, C.D.: 'Voltage Stability of Electric Power System' (Knower Academic, Norwell, MA, 1998)
32 Hemeida, A.M.: 'Improvement of voltage stability and critical clearing time for multi-machine power systems using static VAR compensator', *ICGST-ACSE*, 2009, **9**, (2), pp. 41–47
33 Interconnection for Wind Energy: FERC Stats. & Regs. 31,186 (2005), Order No. 661, 70 Fed. Reg. 34993
34 Wu, Q., Xu, Z., Ostergaard, J.: 'Grid integration issues for large scale wind power plants (WPPs)'. IEEE Power and Energy Society General Meeting, Minneapolis, Minnesota, USA, 25–29 July 2010, pp. 1–7
35 Li, L., Ugrinovskii, V.A.: 'On necessary and sufficient conditions for H_∞ output feedback control of Markov jump linear systems', *IEEE Trans. Autom. Control*, 2007, **52**, (7), pp. 1287–1292

11 Appendix

The sub-optimal control design used in this paper involves solving the optimisation problem given on the right-hand side of (43). Generally, it is difficult to provide a systematic way to perform such optimisation. In this paper, the idea is to replace the problem $\inf_\tau J(\tau, \Theta)$ with an equivalent optimisation problem involving rank constrained LMIs [35]. From (39), we obtain

$$\boldsymbol{A}_i^{\mathrm{T}}\bar{\boldsymbol{X}}_i + \bar{\boldsymbol{X}}_i\boldsymbol{A}_i + \bar{\boldsymbol{C}}_i^{\mathrm{T}}\bar{\boldsymbol{C}}_i - \bar{\boldsymbol{X}}_i[\boldsymbol{B}_i R_i^{-1}\boldsymbol{B}_i^{\mathrm{T}} - \bar{\boldsymbol{B}}_{2_i}\bar{\boldsymbol{B}}_{2_i}^{\mathrm{T}}]\bar{\boldsymbol{X}}_i < 0 \tag{45}$$

by multiplying the left- and right-hand sides of (45) with $\tilde{X}_i = \bar{X}_i^{-1}$, we obtain

$$\tilde{\boldsymbol{X}}_i\boldsymbol{A}_i^{\mathrm{T}} + \boldsymbol{A}_i\tilde{\boldsymbol{X}}_i + \tilde{\boldsymbol{X}}_i\bar{\boldsymbol{C}}_i^{\mathrm{T}}\bar{\boldsymbol{C}}_i\tilde{\boldsymbol{X}}_i - [\boldsymbol{B}_i R_i^{-1}\boldsymbol{B}_i^{\mathrm{T}} - \bar{\boldsymbol{B}}_{2_i}\bar{\boldsymbol{B}}_{2_i}^{\mathrm{T}}] < 0 \tag{46}$$

Introducing matrices $\boldsymbol{F}_i$ of appropriate dimensions, without changing the feasibility of (46), we add a quadratic term of F_i to the left-hand side of (46) as follows

$$\begin{aligned}&\tilde{\boldsymbol{X}}_i\boldsymbol{A}_i^{\mathrm{T}} + \boldsymbol{A}_i\tilde{\boldsymbol{X}}_i + \tilde{\boldsymbol{X}}_i\bar{\boldsymbol{C}}_i^{\mathrm{T}}\bar{\boldsymbol{C}}_i\tilde{\boldsymbol{X}}_i - [\boldsymbol{B}_i R_i^{-1}\boldsymbol{B}_i^{\mathrm{T}} - \bar{\boldsymbol{B}}_{2_i}\bar{\boldsymbol{B}}_{2_i}^{\mathrm{T}}]\\ &+ [F_i^{\mathrm{T}} + \boldsymbol{B}_i R^{-1}]R_i[F_i^{\mathrm{T}} + \boldsymbol{B}_i R_i^{-1}]^{\mathrm{T}} < 0\end{aligned} \tag{47}$$

which is equivalent to

$$\begin{aligned}&\tilde{\boldsymbol{X}}_i\mathbf{A}_i^{\mathrm{T}} + \boldsymbol{A}_i\tilde{\boldsymbol{X}}_i + \tilde{\boldsymbol{X}}_i\bar{\boldsymbol{C}}_i^{\mathrm{T}}\bar{\boldsymbol{C}}_i\tilde{\boldsymbol{X}}_i + \bar{\boldsymbol{B}}_{2_i}\bar{\boldsymbol{B}}_{2_i}^{\mathrm{T}} + F_i^{\mathrm{T}}R_iF_i\\ &+ \boldsymbol{B}_iF_i + F_i^{\mathrm{T}}\boldsymbol{B}_i^{\mathrm{T}} < 0\end{aligned} \tag{48}$$

Using (40), the terms of (48) can be represented as follows

$$\begin{aligned}&\bar{\boldsymbol{B}}_{2_i}\bar{\boldsymbol{B}}_{2_i}^{\mathrm{T}} = \tau_i^{-1}E_iE_i^{\mathrm{T}} + \Theta_i^{-1}L_iL_i^{\mathrm{T}}\\ &\tilde{\boldsymbol{X}}_i\bar{\boldsymbol{C}}_i^{\mathrm{T}}\bar{\boldsymbol{C}}_i\tilde{\boldsymbol{X}}_i = \tilde{\boldsymbol{X}}_i[\boldsymbol{C}_i^{\mathrm{T}}\boldsymbol{C}_i + (\tau_i + \bar{\Theta}_i)H_i^{\mathrm{T}}H_i]\tilde{\boldsymbol{X}}_i\\ &F_i^{\mathrm{T}}R_iF_i = F_i^{\mathrm{T}}[\boldsymbol{D}_i^{\mathrm{T}}\boldsymbol{D}_i + (\tau_i + \bar{\Theta}_i)G_i^{\mathrm{T}}G_i]F_i\end{aligned} \tag{49}$$

Let $\tilde{\tau}_i = \tau_i^{-1}$, $\tilde{\Theta}_i = \Theta_i^{-1}$. By combining (48) and (49), and applying the Schur complement, we obtain the following LMIs with variables $\tilde{X}_i$, F_i, $\tilde{\Theta}_i$, $\tilde{\tau}_i$

$$\begin{bmatrix} Z_i & \tilde{X}_i\boldsymbol{C}_i^{\mathrm{T}} & \boldsymbol{F}_i^{\mathrm{T}}\boldsymbol{D}_i^{\mathrm{T}} & \alpha_i \\ \star & -I & 0 & 0 \\ \star & \star & -I & 0 \\ \star & \star & \star & -\Theta_i \end{bmatrix} < 0 \tag{50}$$

where

$$\begin{aligned}&Z_i = \tilde{\boldsymbol{X}}_i\boldsymbol{A}_i^{\mathrm{T}} + \boldsymbol{A}_i\tilde{\boldsymbol{X}}_i + \tilde{\tau}_iE_iE_i^{\mathrm{T}} + \tilde{\Theta}_iL_iL_i^{\mathrm{T}} + \boldsymbol{B}_iF_i + F_i^{\mathrm{T}}\boldsymbol{B}_i^{\mathrm{T}}\\ &\alpha_i = [F_i^{\mathrm{T}}G_i^{\mathrm{T}} + \tilde{\boldsymbol{X}}_iH_i^{\mathrm{T}}, \ \ldots, F_i^{\mathrm{T}}G_i^{\mathrm{T}} + \tilde{\boldsymbol{X}}_iH_i^{\mathrm{T}}] \quad (N \text{ entries})\\ &\Theta_i = \mathrm{diag}[\tilde{\tau}_iI, \tilde{\Theta}_1I, \ \ldots, \tilde{\Theta}_{i-1}I, \tilde{\Theta}_{i+1}I, \tilde{\Theta}_NI]\end{aligned} \tag{51}$$

Similarly, by substituting (40) into (38) and applying the Schur complement, we obtain the LMIs with variables

$\bar{Y}_i, F_i, \Theta_i, \tau_i$

$$\begin{bmatrix} \beta_i & \bar{Y}_i E_i & \bar{Y}_i L_i \\ \star & -\tau_i I & 0 \\ \star & \star & -\Theta_i I \end{bmatrix} < 0 \tag{52}$$

where

$$\beta_i = \boldsymbol{A}_i^{\mathrm{T}} \bar{Y}_i + \bar{Y}_i \boldsymbol{A}_i - \tau_i \boldsymbol{C}_{yi}^{\mathrm{T}} [D_{yi} \boldsymbol{D}_{yi}^{\mathrm{T}}]^{-1} \boldsymbol{C}_{yi} + \boldsymbol{C}_i^{\mathrm{T}} \boldsymbol{C}_i + (\tau_i + \bar{\Theta}_i) H_i^{\mathrm{T}} H_i$$

The coupling condition $\bar{Y}_i > \bar{X}_i > 0$ is equivalent to

$$\begin{bmatrix} \tilde{X}_i & I \\ I & \bar{Y}_i \end{bmatrix} > 0 \tag{53}$$

Now consider the performance upper bound on the right-hand side of (43). Note that minimising $J(\tau,\Theta)$ is equivalent to minimising $(\lambda_1 + \lambda_2 + \ldots + \lambda_n)$ subject to

$$\lambda_i > x_{i0}^{\mathrm{T}} [\bar{X}_i + \tau_i M_i + \Theta_i \bar{M}_i] x_{i0} \tag{54}$$

Using the Schur complement again, (54) is equivalent to the following LMIs

$$\begin{bmatrix} \lambda_i & \Pi & x_{i0}^{\mathrm{T}} M_i^{1/2} & x_{i0}^{\mathrm{T}} \tilde{M}_i^{1/2} \\ \star & \tilde{X}_i & 0 & 0 \\ \star & \star & \tilde{\tau}_i I & 0 \\ \star & \star & \star & \tilde{\Theta}_i I \end{bmatrix} < 0 \tag{55}$$

here $\Pi = [\pi_1^{1/2} x_{i0}^{\mathrm{T}}, \ldots, \pi_k^{1/2} x_{i0}^{\mathrm{T}}]$. Also the conditions $\tilde{\tau}_i > 0$, $\tau_i > 0$, $\tilde{\tau}_i \tau_i = 1$, $\Theta_i > 0$, $\Theta_i > 0$, $\tilde{\Theta}_i \Theta_i = 1$ are equivalent to the rank constrained LMIs

$$\begin{bmatrix} \tilde{\tau}_i & I \\ I & \tau_i \end{bmatrix} \geq 0, \quad \mathrm{rank} \begin{bmatrix} \tilde{\tau}_i & I \\ I & \tau_i \end{bmatrix} \leq 1 \tag{56}$$

$$\begin{bmatrix} \tilde{\Theta}_i & I \\ I & \Theta_i \end{bmatrix} \geq 0, \quad \mathrm{rank} \begin{bmatrix} \tilde{\Theta}_i & I \\ I & \Theta_i \end{bmatrix} \leq 1 \tag{57}$$

We now consider the following linear cost optimisation problem in the variables λ_i, $\tilde{X}_i$, $\bar{Y}_i$, F_i, $\tilde{\Theta}_i$, $\tilde{\tau}_i$ and τ_i, Θ_i [35]

$$J_{\mathrm{LMI}}^* \triangleq \inf(\lambda_1 + \cdots + \lambda_n) \tag{58}$$

subject to (50), (52), (53), (55)–(57).

doi: 10.1049/iet-gtd.2011.0537